Analysis of Two-Dimensional Airfoil Models as Harvesters of Energy

Luis Gonzaga-Bermeo and Carlos A. Cuenca

1 Introduction

The process of decarbonization of the industry in countries that signed the Paris Agreement of 2008 has promoted the study and development of renewable energy sources as a replacement for fossil fuels. One of the promising concepts is the use of airfoils that describe heave and pitching movements simultaneously [1]. In the present study, two airfoils, one symmetric (NACA0020) and the other asymmetric (NACA1412), are modeled in two dimensions (2D) with the purpose of comparing their efficiencies when these are working in power-extraction regime from an approaching fluid, in this case is water with velocity U_{∞}.

Previous numerical simulations in 2D have been carried out with asymmetric airfoil [2], in laminar regime (100–1000) at different plunging motion profile (sinusoidal and induced), reaching in the best of the cases a maximum efficiency of 20%.

Around this theory of oscillatory airfoils, a hydrokinetic turbine with two airfoils disposed in tandem was tested experimentally in 2009 by Kinsey et al. [3], and the extracted energy compared with conventional rotor blades showed a maximum efficiency greater than 25%.

L. Gonzaga-Bermeo (✉)
DINAVALE, Daule, Ecuador

University of Strathclyde, Naval Architecture, Ocean, & Marine Engineering, Glasgow, UK
e-mail: luis.gonzaga-bermeo.2020@uni.strath.ac.uk

C. A. Cuenca
Facultad de Ingenieria Mecanica y Ciencias de la Produccion, Escuela Superior Politecnica del Litoral, ESPOL, Guayaquil, Ecuador

Department of Naval Architecture and Ocean Engineering, University of São Paulo, São Paulo, Brazil

M. Espinoza-Andaluz et al. (eds.), *Congress on Research, Development and Innovation in Renewable Energies*, Green Energy and Technology,
https://doi.org/10.1007/978-3-030-97862-4_7

This study aims to determine the optimal parameters regarding pitching angle, heaving amplitude, and frequency of oscillation when the airfoils are involved in steady laminar flow (Re 735, Re 1100). In addition, following the recommendation of [2], to ensure that airfoils are operating in power-extraction regime, the feather parameter $\chi = {\theta_0}/{\arctan\left(\frac{\gamma H}{U_\infty}\right)} > 1$ must be applied as necessary condition. This parameter qualifies the effect of the sinusoidal movement of airfoils on the flow regime, where $\theta_0$is the pitching amplitude, H_0 is the heaving amplitude, and $\gamma = 2\pi f$ which is the angular frequency. Hence, the range of values taken is between $1 < \chi < 2.5$, which represent pitching amplitude between $43.32\,^\circ \leq \theta_0 < 90^\circ$. In addition, the effects on varying parameters such as nondimensional frequency $0.11 \leq f^* \leq 0.27$ and heaving amplitude $0.5 \cdot \text{chord} \leq H_0 \leq 1 \cdot \text{chord}$ are investigated.

A mapping of efficiency in the parametric space: pitching amplitude versus nondimensional frequency (f^*, θ_0) is presented for each airfoil when Re = 735, heave amplitude ($H_0 = 1 \cdot$ chord), and pitching axis located at 33% of chord length (C.L.).

In this research, the Eulerian frame of reference is the method used to know the response of the wing when parameters vary. Furthermore, the use of dynamic mesh allowed the deformation of the domain, while the programming in the C language of a user-defined function (UDF) achieved the prescribed oscillatory movement for the airfoils.

Finally, the validation of results is made when contrasting numerical simulation from Kinsey and Dumas with our study at the same chord length of the airfoil (240 mm), symmetric airfoil, Reynolds number of 1100, nondimensional frequency, $f^* = 0.14$, and pitching amplitude of $62.01\,^\circ < \theta_0 < 90^\circ$.

2 Methods

The methodology applied for this study was simulation of the symmetric and asymmetric airfoils at different parameters like nondimensional frequency and amplitude of pitching angle, without considering the angle of attack in the equation of movement. After many simulations (see Table 1), the forces obtained were lifting

Table 1 Range of parameters to evaluate for NACA 0020 and NACA 1412 when fluid velocity in x direction is 0.0030 m/s (Re = 735) and 0.0045 m/s (Re = 1100)

$f^* = \frac{fc}{U_\infty}$	$\omega = 2\pi f$	U_∞	χ	θ_0[rad]	θ_0[deg]
0.11	0.0086394	0.0030 0.0045	$1 < \chi \leq 2.5$	$0.75 \leq \theta_0 < 1.57$	$43.32\,^\circ \leq \theta_0 < 90^\circ$
0.14	0.0109956				
0.16	0.0125664				
0.20	0.0157080				
0.25	0.0196350				
0.27	0.0212058				

force and moment, where both results let us to compute the power efficiency and power extracted. In addition, the authors investigated the influence of the Re number and change of amplitude of heave over the efficiency and power extracted. A flow chart shows the general scheme in Fig. 6. To compare efficiencies when Re number varies, the same parameters in which Kinsey and Dumas found the maximum efficiency were selected.

2.1 Description of Movements

The movement of the airfoils are described as heaving and pitching, in which these movements are simultaneously done with a rotational axis x_p located at 33% chord from the leading edge, as shown in Fig. 1. Equations 1 and 2 describe mathematically the harmonic movements. For heaving, its movement is described with amplitude H_0 which is defined as $1 \cdot \text{chord} = 240$ mm. On another side, angular frequency omega is defined as $\omega = 2\pi \cdot f$, where f is the frequency of oscillation and depends on the operating regime (propulsion or extraction of energy). Finally, the phase angle, Phi, is considered in all simulations as $\phi = 90°$:

$$h(t) = H_0 \sin(\omega t + \phi) \tag{1}$$

For pitching, its movement is around z axis, and the pitching amplitude θ_0 will be varying from $40° < \theta_0 < 90°$. In Eq. 2, the movement is described as a sin function without phase angle:

$$\theta(t) = \theta_0 \sin(\omega t) \tag{2}$$

To know the velocities in heaving and pitching, Eqs. 1 and 2 are derivative respect to time. Therefore, Eqs. 3 and 4 represent these velocities, respectively:

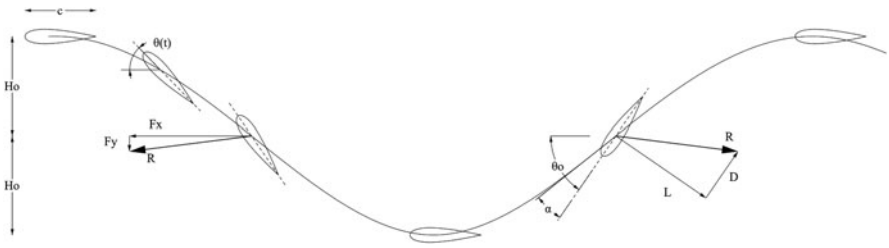

Fig. 1 Representation of oscillatory movement of airfoil. The heave motion follows a sinusoidal function, while the pitching motion is out of phase by 90°. The oncoming water comes from left to right

$$\dot{h}(t) = H_0\, \omega \cos\left(\omega t + \phi\right) \tag{3}$$

The pitching velocity is described in Eq. 4.

$$\dot{\theta}(t) = \theta_0 \omega \cos(\omega t) \tag{4}$$

2.2 Operating Regime for Power Extraction

Power extraction regime is reached when the forces acting on the airfoil, which has imposed movement and upstream flow conditions, such as lift and drag force, have a net force $\vec{R}$ that once decomposed into $\overrightarrow{F_x}$ and $\overrightarrow{F_y}$, the force acting on "y" direction is producing work when the airfoil is heaving while the force acting on "x" direction produces zero work due to angle between vectors $\overrightarrow{F_x}$ and displacement of airfoil $\vec{y}$ is 90°.

In this study, the feathering parameter, χ, is applied as a necessary condition to assure that the airfoil is working in power-extraction regime [4]:

$$\chi = \frac{\theta_0}{\arctan\left(\frac{H_0 \omega}{U_\infty}\right)} \tag{5}$$

That is when $\chi > 1$ and the angle of attack which is constant is $\alpha_{T/4} < 0$. As consequence, using Equation 5, the pitching amplitude, θ_0, is defined as:

$$\theta_0 = \chi \cdot \arctan\left(\frac{H_0 \omega}{U_\infty}\right) \tag{6}$$

The range of pitching amplitude, θ_0, when $0.11 \leq f^* \leq 0.27$ is shown in Table 1.

2.3 Power and Efficiency

The power extracted per unit of depth is produced by vertical force, $F_y(t)$ and velocity when heaving $V_y(t)$, also by the Torque, $M(t)$, about the axis x_p and angular velocity $\dot{\theta}(t)$:

$$P = P_y(t) + P_\theta(t) = F_y(t)\, V_y(t) + M(t)\, \dot{\theta}(t) \tag{7}$$

Then for calculation of efficiency, the total power available P_a from oncoming water flow through the extraction plane is calculated as follows:

$$P_{\mathrm{a}} = \frac{1}{2}\rho U_{\infty}^{3}\, d \tag{8}$$

where U_∞ is the velocity of flow, ρ is the water density (999 kg/m^3), and "d" is the overall extent of airfoil when it moves in y direction.

The efficiency is defined as the ratio of the cycle-average power extracted ($\overline{P}$) to the total power available P_{a}:

$$\eta = \frac{P_y(t) + P_\theta(t)}{\frac{1}{2}\rho U_{\infty}^{3}\, d\, s} \tag{9}$$

Usually, the power extraction efficiency maximum value is about 59% from the Betz analysis of a stationary inviscid stream tube around a power-extraction device [5].

2.4 Geometrical Model

The geometry of domain, as well as the symmetrical and nonsymmetrical airfoils, was modeled in rhinoceros, [6]. The airfoils have the same chord length of 240 mm, measured from leading edge to the trailing edge. The distance from leading edge to inlet is given in terms of chord length (10 · chord), the same with the distance from trailing edge to outlet (16 · chord), and finally, from top or bottom of airfoil to symmetry (see Fig. 2). The initial position of wing is at (7 · chord) from upper symmetry to top surface of airfoil, while the lowest position of airfoil is when it reaches (7 · chord) from bottom symmetry to bottom surface of airfoil, that is when $t/T = 0.5$. The airfoil is moving vertically in the range $0.5 \leq \frac{H_0}{\text{chord}} \leq 1$.

The dimension of the domain is given so that there is no interference between the movement of the folio and the control surface, in addition to guaranteeing the capture of the wake of the airfoil. This was verified by observing the velocity vectors in the near parts of the symmetry zones of some of the analyzed models, identifying that they remain parallel to said symmetry contours.

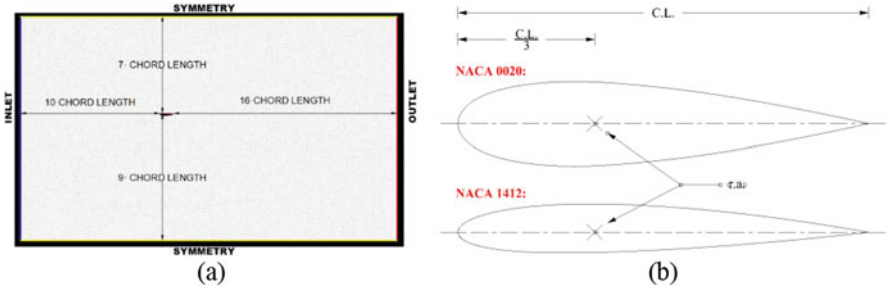

Fig. 2 (**a**) Dimension of domain and (**b**) upper airfoil NACA 0020 and bottom NACA 1412 geometries with chord length (C.L.) 240 mm

2.5 Numerical Model

After modeling in rhinoceros, the domains and airfoils were exported into Ansys Fluent [7]. For NACA 0020, five types of meshes were used to guarantee independence of results, (see Table 2).

From this table, the coarse mesh has 21 k nodes, medium mesh has 61 K nodes, and fine mesh has 201 k nodes. The selection of the mesh followed the flow chart given at left side of Fig. 6.

2.5.1 Meshing and Mesh Independence Analysis

For each type of mesh considered, both the external limits and the edge of the profile analyzed have been refined, increasing the refinement in the area close to the border of the airfoil. In this way, elements of the linear triangular type have been used to discretize the area of interest. In addition, layers of quadrangular elements were used in the inflation option around the wall surface, as shown in Fig. 3. In all cases, it was ensured that the aspect ratio of the generated elements is not greater than three to avoid discontinuity errors. To achieve this, the height of the first element was calculated using the theory of Y^+ for laminar flows, which allows to determine the appropriate size of element height in the area near the wall of the airfoil [8].

To verify the mesh size selected during the analysis, the value corresponding to the area obtained under the curve (area under the curve, AUC) which represents "Lift vs. t" is used. This is achieved by verifying that the area under the selected curve does not change drastically when obtaining responses with different meshes as shown in Fig. 4, which is used due to these let us determine the efficiency of the airfoils.

This means that when the mesh is refined, in this case, with 201 K nodes, it does not produce a variation of results greater than 7% when the mesh has 21 K nodes as observed in Fig. 4c. Therefore, considering the difference in computational analysis shown in Table 2, it can be concluded that a numerical model with a mesh of approximately 21 K nodes allows obtaining a result as significant as a much more

Table 2 Summary of meshing

Type of mesh	Number of nodes	Size of elements around the wall [mm]	Size of elements on domain [mm]	Time for processing [h]
Mesh 1	6000	4.00	200	4
Mesh 2	21,000	1.50	100	10
Mesh 3	43,000	1.50	50	12
Mesh 4	61,000	0.47	100	77
Mesh 5	201,000	1.00	12.5	168

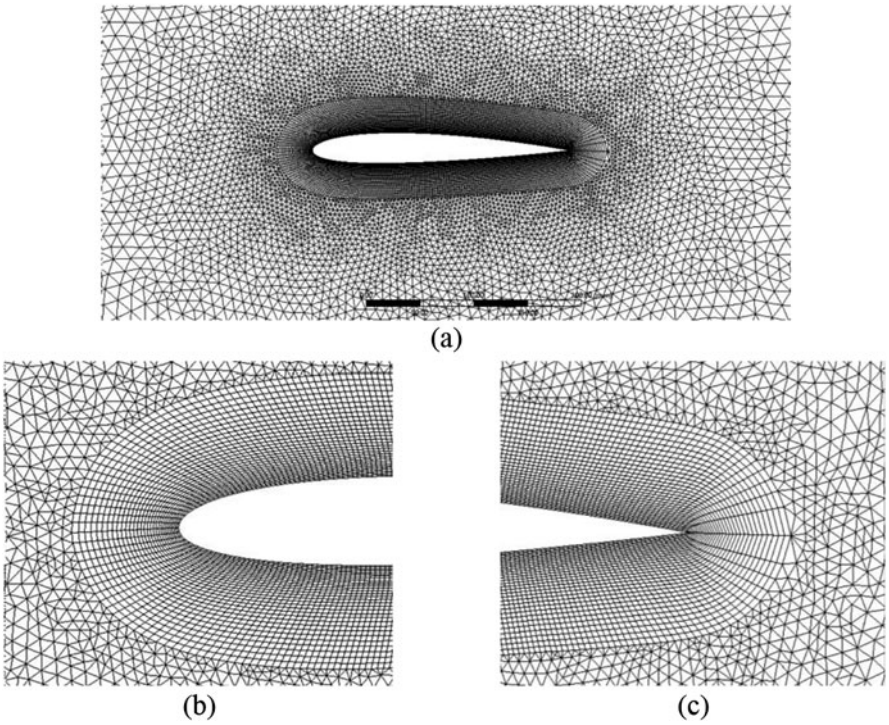

Fig. 3 (**a**) Mesh around the airfoil, (**b**) mesh detail on leading edge, and (**c**) mesh detail on trailing edge

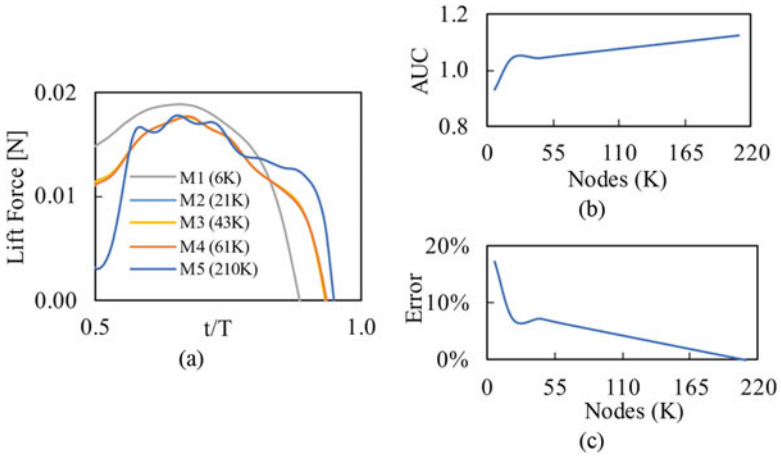

Fig. 4 (**a**) Lift curves (RLC) per each mesh's quality, (**b**) area under the curve for each RLC per each mesh's quality, and (**c**) relative error of calculation of AUC for each lift curve measured between 0.5 and 1 T

refined mesh. Finally, according to the results obtained, the type of numerical discretization defined for mesh type 2 is selected for the models to be analyzed for both the symmetric and asymmetric airfoils.

2.5.2 Boundary Conditions and Loads

In this study, the fluid moves in laminar state from left to right at $V_x = 0.003$, ($R_e = 735$). The *Inlet BC* is located at the left side of airfoil leading edge at $10 \cdot \text{chord} = 2400$ mm. On another hand, the *Outlet BC* is located at $16 \cdot \text{chord} = 3840$ mm, measured from trailing edge to right side of domain. Its distance is far away from the airfoils in order to not affecting the developed state of flow [9, 10].

The exit pressure was defined as "*gauge pressure*" equal to zero. After that, the *wall BC* applied to airfoil profiles (solid wall) is no-slip condition ($v_x = v_y = 0$); this is based on viscosity of boundary layer theory. Finally, but not less important, symmetry condition is applied to upper and bottom edge of domain based on there is no flow across these boundaries $\left(\vec{v} \cdot \vec{n} = 0\right)$.

2.5.3 Dynamic Mesh, User-Defined Function

The dynamic mesh selected method is diffusion-based smoothing which is recommended when there is large deformation of mesh and involves rotational movement. Although this method is computationally costly than spring-based smoothing, diffusion-based generates better quality meshes [11]. The formulation for the diffusion coefficient selected is boundary distance: $\gamma = \frac{1}{d^{\xi}}$ where d is the normalized boundary (0.50 mm) and ξ, the diffusion parameter, is taken as 1.5, due to high values (0–2) preserve the mesh close the moving boundary. Thanks to the programming of a user-defined function (UDF), the symmetric and nonsymmetric airfoils can move in heaving and pitching following the equation of movements 1 and 2.

After many simulations, it was demonstrated that after the first period, the forces did not change, as shown in Fig. 5. As consequence, only two cycles were simulated, which permitted reduction of the computational process time. On another hand, the time step was defined using Courant-Friedrichs-Lewy condition $\text{CFL} = \frac{U_\infty \Delta t}{\Delta h} \tilde{1}$, where Δh is the size of the cell, measured horizontally around the airfoil, and Δt is the time step.

Table 3 shows the CFLs for the f^* that allow obtaining efficiencies greater than zero.

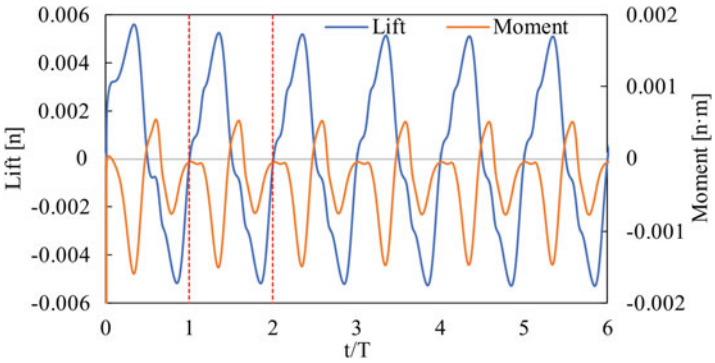

Fig. 5 Stability of periodic response for lift force by moment

Table 3 Summary of CFL, time step, period in one cycle, and number of time steps for two cycles

f^*	Frequency	CFL	Δt [s]	T[s]	N° time steps in 2 T
0.11	0.00138	1.00	0.167	727.27	8731
0.14	0.00175	1.00	0.167	571.43	6860
0.16	0.00200	0.9996	0.167	500.00	6006

2.5.4 Solver and Residuals

The model to solve Navier–Stokes equation is laminar model [12], while the numerical solution was computed with finite volume method using the SIMPLE scheme. The time-stepping is second-order upwind scheme.

On another side, the effect of convergence of the value for the residual was analyzed, where it verified that residual of 10^{-3} produced the same response as 10^{-8}; hence, this value was adopted for all simulations that allow the optimization of computational process time [13].

Finally, two airfoils were analyzed with two flow velocities of 0.003 m/s and 0.0045 m/s, at different values of f^* as shown in Table 1. The velocity 0.0045 m/s (Re = 1100) is used to validate results with previous literature.

To summarize the methodology applied, the flow chart of Fig. 6 at the left side presents how the mesh was selected, while at the right side is showing what forces are calculated once parameters like Re, nondimensional frequency, and pitching amplitude were set. Then the results of efficiency are printed only when it is positive.

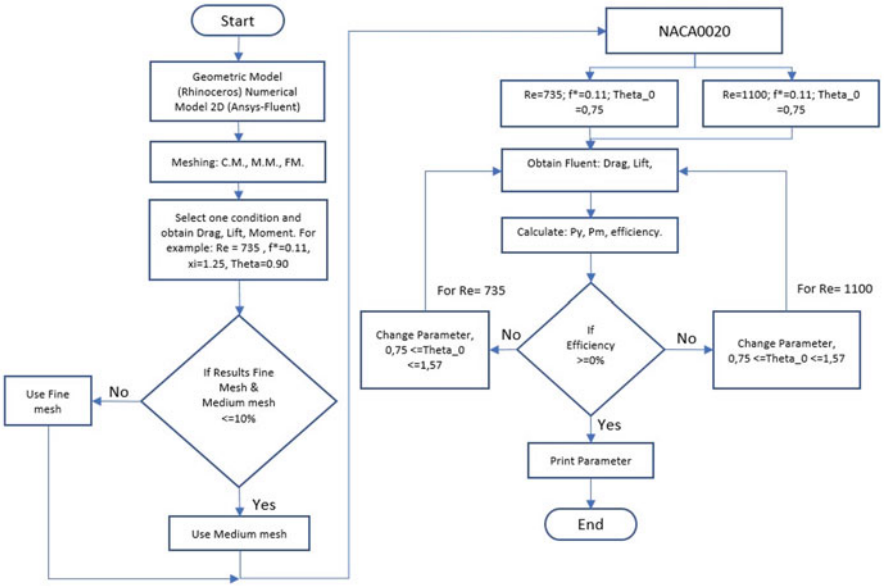

Fig. 6 Flowchart process

3 Results

3.1 Forces Acting on NACA 0020 Versus NACA 1412

Lift force and moment were used to calculate the power where it was found that lift force contributed more than moment. On another hand, while the airfoil is extracting energy, the drag force is greater than zero. After calculating the extracted power using Eq. 7, the efficiency was calculated using the average power of one period. In Table 7, the summary of efficiencies for the airfoils NACA 0020 are NACA 1412 are shown.

3.2 Extract of Energy and Efficiency on NACA 0020 Versus NACA 1412

The simulations were carried on for $0.11 \leq f^* \leq 0.27$, and for amplitude of pitching angles between $43.32^\circ \leq \theta_0 < 90^\circ$, the angle of attack was not considered on these simulations as a fixed parameter neither variable. Therefore, the results showed that maximum efficiencies for symmetric airfoil is reached when $f^* = 0.14$ and $\theta_0 = 62.01^\circ$, while for $f^* > 0.16$, the values of efficiencies turn into negative showing that these parameters should be omitted when extracting power. In addition, when

Table 7 Summary of efficiency with pitching angle $43.32\,^{\circ} < \theta_0 < 90^{\circ}$ at $Re = 735$

NACA	θ_0	$f^* = 0.11$	$f^* = 0.14$	$f^* = 0.16$	$f^* = 0.20$	$f^* = 0.25$	$f^* = 0.27$
0020 (1412)	43.32	0.89% (3.92%)	0.79% (−4.80%)	−15.34% (−13.35%)	−42.42% (−38.66%)	−95.08% (−92.79%)	−118.39% (−119.08%)
0020 (1412)	51.98	4.04% (12.34%)	2.42% (5.36%)	−3.08% (−0.79%)	−20.71% (−17.78%)	−57.96% (−51.64%)	−76.14% (−70.26%)
0020 (1412)	62.01	10.29% (16.42%)	11.31% (13.66%)	7.30% (9.63%)	−11.90% (−2.67%)	−29.96% (−26.24%)	−42.06% (−38.26%)
0020 (1412)	72.34	6.56% (9.27%)	9.27% (10.55%)	6.38% (7.16%)	−3.10% (−1.17%)	−24.64% (−21.32%)	−35.63% (−32.04%)
0020 (1412)	77.97	0.10% (1.77%)	2.04% (2.93%)	−1.03% (−1.43%)	−12.68% (−11.63%)	−34.34% (−31.10%)	−46.78% (−42.11%)
0020 (1412)	84.90	−11.12 (−10.44%)	−11.40% (−12.67%)	−16.52% (−22.08%)	−34.32% (−36.79%)	−64.43% (−61.81%)	−80.28% (−74.20%)
0020 (1412)	90.00	−20.60% (−21.36%)	−25.88% (−28.22%)	−32.71% (−37.26%)	−59.82% (−63.54%)	−98.53% (−99.57%)	−119.11% (−116.44%)

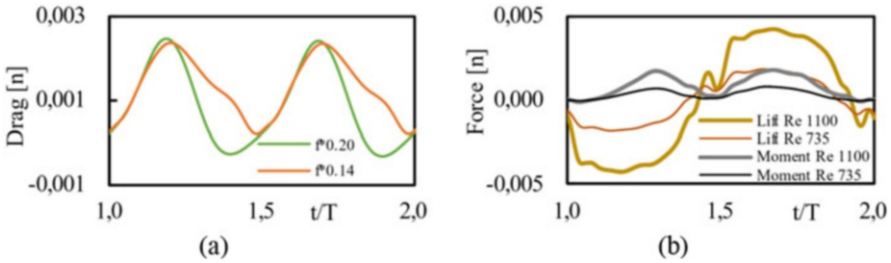

Fig. 7 (**a**) Drag force for NACA 0020 at $0.11 \leq f^* \leq 0.2$ at $\theta_0 = 62.01°$. (**b**) Lift and moment responses for symmetric airfoil at $\theta_0 = 62.01°$

Table 4 Efficiencies for symmetric and asymmetric airfoils at $\theta_0 = 72°$ and $f^* = 0.16$

Airfoil	Re = 735	Re = 1100
Symmetric	26.08%	19.54%
Asymmetric	17.80%	22.90%

$f^* \leq 0.16$, the amplitude pitching angle plays an important role due to when angle is less than 60° and greater than 70° the efficiencies are less than 10%.

For the asymmetric airfoil NACA 1412, the maximum efficiency is reached when $f^* = 0.16$ with $\theta_0 = 62.01°$. Furthermore, the efficiency values are positive when $f^* \leq 0.16$ and amplitude of pitching angle $62.01° \leq \theta_0 \leq 72.34°$.

Another important characteristic that is shown in Table 7 is that after reaching the peak of efficiency, it decreases. Besides, Reynolds number also has influence on the efficiency due to it was found that at higher value, Re 1100, the efficiency grew up to 2.6% and nondimensional frequency decreases 0.03 which suggest that at higher *Re*, the efficiency improve when the angular frequency reduces. According to [1] at large flow, probably the Re reduces the effective thickness of the airfoil and increases the force generation, as shown in Fig. 7b.

In addition, when evaluating the efficiency when the ratio H_0/chord = 0.5, it is observed that the efficiency increases for asymmetric airfoil but not for symmetric one, as observed in Table 4. The main reason is because the authors assumed that by applying Kinsey and Dumas numerical simulation parameters ($\theta_0 = 72°$ and $f^* = 0.16$), they would get maximum efficiencies which is not necessarily true.

On another hand, the average extracted power when Re 735, in one cycle, is calculated when the maximum efficiency is reached. For example, in the symmetric airfoil, the average power in one cycle is 5.23E − 10 [KWh] when $f^* = 0.14$, $\theta_0 = 62.01°$, while for Re 1100 the average power is 3.13E - 9 [KWh]. This, in turn, represents 598% of increment. For asymmetric airfoil, the average power is 8.65E - 10 [KWh], $f^* = 0.11$, and $\theta_0 = 62.01°$, and for Re = 1100 the average

Table 5 Efficiencies and extracted power for each NACA airfoil at different Re at $\frac{H_0}{c} = 1$

Airfoil – $H_0/c = 1$	Re = 735	Re = 1100
NACA 0020	11.31% 5.23E-10 [KWh] ($f^* = 0.14$; $\theta_0 = 62.01°$)	13.93% 3.13E-09 [KWh] ($f^* = 0.11$; $\theta_0 = 62.01°$)
NACA 1412	16.42% 8.65E-10 [KWh] ($f^* = 0.11$; $\theta_0 = 62.01°$)	17.14 4,74E-09 [KWh] ($f^* = 0.11$; $\theta_0 = 62.01°$)

Table 6 Efficiencies and extracted power for each NACA airfoil at different Re at $\frac{H_0}{c} = 0.5$

Airfoil – $H_0/c = 0.5$	Re = 735	Re = 1100
NACA 0020	26.08% 1.39E-09 [KWh] ($f^* = 0.14$; $\theta_0 = 62.01°$)	19.54% 3.08E-09 [KWh] ($f^* = 0.11$; $\theta_0 = 62.01°$)
NACA 1412	17.80% 5.10E-10 [KWh] ($f^* = 0.11$; $\theta_0 = 62.01°$)	22.90% 4.24E-09 [KWh] ($f^* = 0.11$; $\theta_0 = 62.01°$)

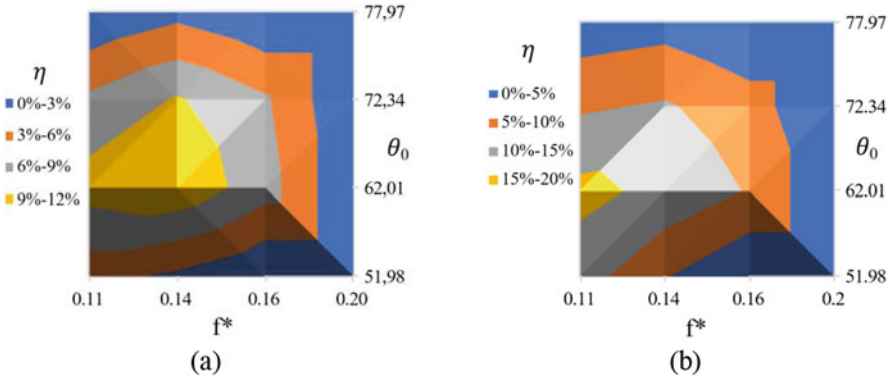

Fig. 8 Efficiency at $0.11 \leq f^* \leq 0.2$ at $\theta_0 = 62.01°$ for: (**a**) NACA 0020, (**b**) NACA 1412

power is 4.74E - 09 [KWh] same f^* and θ_0 what means 548% of increment. In Tables 5 and 6, the reader can observe the improvement of working at different *Re* number and reduced heave amplitude.

Figure 8 shows the maximum efficiency values for each airfoil analyzed in a mapping of efficiencies in the space (f^*, θ_0).

3.3 Validation of Results

The validation of results is done when the authors compare the trend of the results for the efficiencies and amplitude of pitching angle θ_0 with Kinsey-Dumas literature, [4], where higher efficiencies are reached when $f^* < 0.18$ and $60 < \theta_0 < 80°$.

4 Discussion

For the analyses carried out, computers whose computing capacity corresponds to Core i7 processor, 8 cores, and 16 GB of RAM with AMD Radeon HD 7000 graphics card were used in which the calculations could be performed in an average of 10 hours.

It was numerically verified that the results had minimum error when modifying parameters such as the number of nodes in the selected mesh. In addition, when the tolerance in the residuals is reduced, the computational processing time was improved.

It was analyzed that the results obtained did not vary for different mesh changes, obtaining that with models of 21 K nodes, the responses were less than 7% for the models of 210 K nodes. That confirmed that the responses are independent with the selected mesh.

5 Conclusions and Recommendations

From the results obtained, the following can be observed:

1. The geometry of the airfoils affects the efficiency obtained, where this value with the asymmetric type airfoil presents an efficiency 2.62% greater than that obtained with symmetric airfoil as stated in [1].
2. The calculations presented in the present investigation were carried out without considering an angle of attack in the rotational motion equation, that is, $\alpha = 0$. Likewise, the simulation was carried out for $=1100$, $f^* = 0.12$, $\theta_0 = 62°$, and $\alpha = 23°$ with which it was observed that there is an increase in efficiency, which shows the importance of including this value within the equation of motion to improve efficiency.
3. It was found that the efficiency of the two airfoils increases when the value of the $H_0/chord$ ratio decreases from 1 to 0.5, as well as increases when the Re increases.
4. The power generation is very small. Consequently, changes must be implemented to the magnitudes of airfoil geometry, and thus, analyze if the efficiency increases. Besides, the 3D analysis of these must be carried out to identify any change in the results.

Recommendations for future work are the following:

1. To add the value of the angle of attack to increase the power and efficiency obtained for the airfoils.
2. To analyze the airfoils considering their three dimensions. In addition, the variations on the H_0/chord ratio and at different frequencies $f^* < 0.20$ with $\Delta f^* = 0.01$, values of $60^\circ \leq \theta_0 \leq 80^\circ$ with $\Delta\theta = 2^\circ$, to determine the response of these changes and generate a space of efficiencies, $\eta(f^*, \theta_0)$, more detailed.
3. To analyze the pressure coefficient along the chord and the effect of the leading-edge vortex shredding.

References

1. Xiao, Q., & Zhu, Q. (2014, April). A review on flow energy harvesters based on flapping foils. *Journal of Fluids and Structures, 46*, 174–191. https://doi.org/10.1016/j.jfluidstructs.2014.01.002
2. Zhu, Q. (2011, May). Optimal frequency for flow energy harvesting of a flapping foil. *Journal of Fluid Mechanics, 675*, 495–517. https://doi.org/10.1017/S0022112011000334
3. Kinsey, T., et al. (2011, June). Prototype testing of a hydrokinetic turbine based on oscillating hydrofoils. *Renewable Energy, 36*(6), 1710–1718. https://doi.org/10.1016/j.renene.2010.11.037
4. Kinsey, T., & Dumas, G. (2008, June). Parametric study of an oscillating airfoil in a power-extraction regime. *AIAA Journal, 46*(6), 1318–1330. https://doi.org/10.2514/1.26253
5. Betz, A. (2013, August). The maximum of the theoretically possible exploitation of wind by means of a wind motor. *Wind Engineering, 37*(4), 441–446. https://doi.org/10.1260/0309-524X.37.4.441
6. McNeel, R., et al. (2010). *Rhinoceros 3D, Version 6.0*. Robert McNeel & Associates.
7. Swanson, J. (2020). *Ansys, 2020 R1*. NASDAQ. [Online]. Available: https://www.ansys.com/academic/students
8. Cadence. (2020). Compute Grid Spacing for a Given Y+. *pointwise.com*. https://www.pointwise.com/yplus/index.html. Accessed 23 July 2021.
9. Versteeg, H. K., & Malaladekera, W. (2007). *An introduction to computational fluid dynamics* (2nd ed.). Pearson Prentices Hall.
10. Blazek, J. (2015). *Computational fluid dynamics: Principles and applications* (3rd ed.). Elsevier.
11. Ansys Training. (2019). *Ansys fluent dynamic mesh modeling*. Virtual – WebEx. [Online]. Available: https://www.ansys.com/training-center/course-catalog/fluids/ansys-fluent-dynamic-mesh-modeling
12. ANSYS Inc. (2013). *Ansys fluent theory guide* (15th ed.). ANSYS.
13. ANSYS Inc. (2012). Monitoring residuals. In *ANSYS FLUENT 12.0 User's guide*. https://www.afs.enea.it/project/neptunius/docs/fluent/html/ug/node812.htm. Accessed 1 Sept 2021